# Determining the Sources and Transport of Brown Carbon Using Radionuclide Tracers and Modeling

Hongxing Jiang[1], Jun Li[1], Rong Sun[1], Guoqing Liu[2], Chongguo Tian[3], Jiao Tang[1], Zhineng Cheng[1], Sanyuan Zhu[1], Guangcai Zhong[1], Xiang Ding[1], and Gan Zhang[1]

[1]Guangzhou Institute of Geochemistry
[2]Shenzhen University
[3]Yantai Institute of Coastal Zone Research

November 22, 2022

**Abstract**

The isotope tracer technique plays a key role in identifying the sources and atmospheric processes affecting pollution. The sources of brown carbon (BrC) at Guangzhou during 2017-2018 was characterized by positive matrix factorization with carbon isotope constraints and multiple linear regression analysis. The primary emission factors of fossil fuel combustion (FF) and biomass burning (BB) accounted for 34% and 27% of dissolved BrC absorption at $\lambda$ = 365 nm, respectively. The total mean light absorption contributed by secondary sources was 39%. The absorption of FF-origin BrC was relatively stable and dominant in the summer monsoon period, whereas the absorption of BrC from BB and secondary nitrate formation increased and contributed larger fractions during the winter monsoon period. Transported BrC was estimated using an index of 7 Be/(7 Be+n 210 Pb). Higher values were generally accompanied by lower BrC absorption, whereas lower values were associated with higher BrC absorption, indicating that BrC absorption of aerosols transported from the upper-atmosphere is lower than that of aerosols transported near the surface. Based on the positive correlations between 210 Pb and BrC absorption and non-fossil dissolved organic carbon in the winter monsoon period, we estimated that the contribution of invasive BrC (include ground and upper-atmosphere level) to total absorption during the period of elevated BrC was approximately 50%, which was likely related to BB organic aerosols and secondary nitrate formation processes. This study supports radionuclides as a novel method for characterizing the sources and transport of BrC that can be applied in future atmospheric research.

# Determining the Sources and Transport of Brown Carbon Using Radionuclide Tracers and Modeling

**Hongxing Jiang[1,2,3,4], Jun Li[*,1,2,3], Rong Sun[1,2,3,4], Guoqing Liu[5], Chongguo Tian[6], Jiao Tang[1,2,3], Zhineng Cheng[1,2,3], Sanyuan Zhu[1,2,3], Guangcai Zhong[1,2,3], Xiang Ding[1,2,3], Gan Zhang[1,2,3]**

[1]State Key Laboratory of Organic Geochemistry and Guangdong province Key Laboratory of Environmental Protection and Resources Utilization, Guangzhou Institute of Geochemistry, Chinese Academy of Sciences, Guangzhou, 510640, China

[2]CAS Center for Excellence in Deep Earth Science, Guangzhou, 510640, China

[3]Guangdong-Hong Kong-Macao Joint Laboratory for Environmental Pollution and Control, Guangzhou Institute of Geochemistry, Chinese Academy of Science, Guangzhou 510640, China

[4]University of Chinese Academy of Sciences, Beijing, 100049, China.

[5]Department of Nuclear Science and Technology, College of Physics and Engineering, Shenzhen University, Shenzhen, 518060, China

[6]Key Laboratory of Coastal Environmental Processes and Ecological Remediation, Yantai Institute of Coastal Zone Research, Chinese Academy of Sciences, Yantai, 264003, China

Corresponding author: Jun Li (junli@gig.ac.cn)

**Key Points:**

- Source apportionment of atmospheric DOM in Guangzhou were performed by using $^{14}C$-constrained PMF model
- PMF-based MLR analyses show that BrC increased during winter with the transportation of BBOA and secondary nitrates formation processes
- $^{210}Pb$-based estimation reveal that the transport BrC accounted for approximately 50% of total BrC absorption during winter monsoon

## Abstract

The isotope tracer technique plays a key role in identifying the sources and atmospheric processes affecting pollution. The sources of brown carbon (BrC) at Guangzhou during 2017-2018 was characterized by positive matrix factorization with carbon isotope constraints and multiple linear regression analysis. The primary emission factors of fossil fuel combustion (FF) and biomass burning (BB) accounted for 34% and 27% of dissolved BrC absorption at $\lambda = 365$ nm, respectively. The total mean light absorption contributed by secondary sources was 39%. The absorption of FF-origin BrC was relatively stable and dominant in the summer monsoon period, whereas the absorption of BrC from BB and secondary nitrate formation increased and contributed larger fractions during the winter monsoon period. Transported BrC was estimated using an index of $^{7}Be/(^{7}Be+n^{210}Pb)$. Higher values were generally accompanied by lower BrC absorption, whereas lower values were associated with higher BrC absorption, indicating that BrC absorption of aerosols transported from the upper-atmosphere is lower than that of aerosols transported near the surface. Based on the positive correlations between $^{210}Pb$ and BrC absorption and non-fossil dissolved organic carbon in the winter monsoon period, we estimated that the contribution of invasive BrC (include ground and upper-atmosphere level) to total absorption during the period of elevated BrC was approximately 50%, which was likely related to BB organic aerosols and secondary nitrate formation processes. This study supports radionuclides as a novel method for characterizing the sources and transport of BrC that can be applied in future atmospheric research.


## 1 Introduction

Atmospheric brown carbon (BrC) has gained attention over the past decades due to its significant impact on the radiative balance of the earth, which may cause uncertainties in global radiative forcing estimation[*Andreae and Gelencsér*, 2006; *Hecobian et al.*, 2010; *Ramanathan et al.*, 2005; *Wang et al.*, 2014]. Biomass burning (BB) has been identified as an important source of BrC in laboratory experiments[*Chen and Bond*, 2010; *Lin et al.*, 2016; *Sengupta et al.*, 2018; *Xie et al.*, 2019a]. Many studies of regional hot spots, such as the Indo-Gangetic Plain in South Asia[*Bikkina et al.*, 2017; *Gustafsson et al.*, 2009], East Asia[*Desyaterik et al.*, 2013; *Kirillova et al.*, 2014a; *Yan et al.*, 2015], and the Amazon Basin[*Mok et al.*, 2016; *Rizzo et al.*, 2011], have demonstrated that atmospheric BrC is largely derived from the consumption of biomass fuels and regional forest fires. However, BrC also originates from sources other than BB, such as fossil fuel combustion (FF)[*Healy et al.*, 2015; *Olson et al.*, 2015; *Yan et al.*, 2017] and the secondary formation of biogenic and anthropogenic volatile organic compounds (VOCs)[*Liu et al.*, 2016; *Nguyen et al.*, 2013; *Xie et al.*, 2017a], complicating BrC source apportionment in the actual atmosphere. Furthermore, the phenomenon of long-range BrC transport has been widely observed and reported. For example, the long-range transport of BB organic aerosols (BBOA) can result in BrC occurrence in urban areas[*Healy et al.*, 2015; *Liu et al.*, 2019; *Wang et al.*, 2019b], plateau regions[*Wang et al.*, 2018; *Wang et al.*, 2019c], and arctic areas[*Barrett and Sheesley*, 2017; *Stohl et al.*, 2006], where BB events are unlikely to occur. However, a recent study noted the nearly complete loss of BrC during the transport of wildfire aerosols (>7000 km away within about two weeks), indicating a very minor direct radiative effect of wildfire BrC on the global average[*Zheng et al.*, 2020]. Thus, estimating the contributions of transported BrC is important for radiative forcing modeling at regional and

global scales[*Ramanathan et al.*, 2007]. Hitherto, few studies had reported the contributions of regionally transported BrC at observation sites.

Generally, previous studies have used organic tracers, inorganic ions, and radiocarbon as indicators to qualitatively explain the sources of BrC[*Huang et al.*, 2018; *Kirillova et al.*, 2014a; *Kirillova et al.*, 2014b; *Wu et al.*, 2019; *Yan et al.*, 2015]. Recently, BrC source apportionment has been performed using on-line aerosol mass spectrometry based on positive matrix factorization (PMF) solutions of aerosol chemical composition combined with multiple linear regression (MLR) models[*Qin et al.*, 2018; *Wang et al.*, 2019b; *Washenfelder et al.*, 2015]. Each of these methods has its limitations, and the accuracy and credibility of the results depend largely on the accuracy of organic aerosol source apportionment. For example, the chemical species used as PMF inputs always have multiple sources and may be unstable, which could lead to underestimation[*Gensch et al.*, 2018; *Zong et al.*, 2016]. Atmospheric carbon isotopes provide useful information about the source types, chemical aging, and regional transport of organic carbon (OC). The radiocarbon ($^{14}C$) method is a powerful technique for analyzing the sources of fossil (e.g., coal and liquid FF) and non-fossil (e.g., biogenic emissions and BB) carbon[*Szidat*, 2009]. Recent studies have indicated that the offline PMF method coupled with $^{14}C$ analysis could provide clear insights into the source apportionment of water-soluble OC[*Huang et al.*, 2014; *Zhang et al.*, 2018].

The effects of long-range dynamic transport can be estimated using two naturally occurring radionuclide tracers, beryllium-7 ($^{7}Be$) and lead-210 ($^{210}Pb$). The natural cosmogenic radionuclide $^{7}Be$, with a half-life of 54 days, is produced in the stratosphere and upper troposphere via spallation of atmospheric carbon, oxygen, and nitrogen. $^{210}Pb$ has a longer half-life of 22.3 years and is the decay product of gaseous radon-222. Radon-222 is almost entirely produced from radium, which is ubiquitously present in soils, with marine systems contributing only 1% of soil-emitted radon-222 to the atmosphere[*Grossi et al.*, 2016; *Lin et al.*, 2014]. These two radionuclides are immediately attached to submicron aerosol particles after entering the atmosphere and are removed mainly through depositional processes. The unambiguous sources and stable chemical properties make these radionuclides useful indicators of continental transport and the stratosphere-troposphere exchange processes affecting submicron aerosols[*Grossi et al.*, 2016; *Hammer et al.*, 2007; *Lin et al.*, 2014].

Lying below the Tropic of Cancer and on the coast of South China, Guangzhou (GZ) has a typical monsoon-controlled climate that is mainly affected by marine and continental air masses, with wet and hot conditions in summer (summer monsoon, marine air mass dominant) and dry and cool conditions in winter (winter monsoon, continental air masses dominant). In particular, the geographical location and climate of GZ provides a unique opportunity to assess how long-range transport impacts the light-absorption properties of BrC. In this study, (1) a carbon-isotope-based method and the PMF-MLR model are coupled to quantitatively differentiate and identify the sources of total soluble BrC in the atmosphere; and (2) the factors that influence the BrC transported to the observation site were estimated using $^{210}Pb$ and $^{7}Be$. Our findings provide new insights into the sources of BrC, including local emissions and regional transport, and the contributions of transported BrC are estimated based on $^{210}Pb$ for the first time.

## 2 Experiments and Methods

### 2.1 Sampling and Pretreatment.

Sampling was conducted from July 2017 to June 2018 at the Guangzhou Institute of Geochemistry (GIG), an urban site in GZ with no obvious point emission sources nearby[*Liu et al.*, 2014]. Ambient particulate matter ($PM_{2.5}$) samples were collected on prebaked quartz fiber filters (MK360, 20.3 × 25.4 $cm^2$; Munktell; preheated at 450°C for 6 h before use and weighed) over a period of 24 h with a high-volume air sampler (Shanghai XTrust Analytical Instruments Co., Ltd.) at a flow rate of 1 $m^3 \cdot min^{-1}$. Filters were wrapped with prebaked aluminum foil, sealed, and stored in a −20°C freezer.

A total of 55 samples were selected for analysis (Table S1). The entire filters were extracted three times in 50 mL methanol for 30 min and concentrated with a rotary evaporator to approximately 3–4 mL. The extracts were then transferred to pre-weighed clean bottles and weighed the extracts. The extracts were stored at 4°C until further analysis and are defined as dissolved organic matter (DOM) in this study.

### 2.2 Chemical Species Analysis and Light Absorption Measurement.

The methods used for the analysis of DOM, organic and elemental carbon (OC and EC), water-soluble ions ($Na^+$, $NH_4^+$, $K^+$, $Cl^-$, $SO_4^{2-}$, $NO_3^-$)[*Mo et al.*, 2018; *Mo et al.*, 2017], monosaccharides (levoglucosan, mannosan, galactosan)[*Jiang et al.*, 2018], organic tracers of secondary organic aerosols (SOA)[*Li et al.*, 2013], polycyclic aromatic hydrocarbons (PAHs), and n-alkanes[*Geng et al.*, 2020; *Mao et al.*, 2018] were similar to those reported in previous studies and details are provided in Text S1 and Table S2. Approximately 1/20 of the total mass of DOM was transferred and brought to a volume of 15 mL. After filtering through 0.22-μm hydrophobic polytetrafluoroethylene membranes, the light-absorption spectra of the DOM were obtained using an ultraviolet (UV)-visible spectrometer (UV-4802; Unico) over the range of 250–800 nm at an interval of 0.5 nm with an accuracy of 10 nm. Prior to analysis, the corresponding solvent was analyzed to obtain a zero value for abundance. The absorbance of field blank sample extracts was also measured and subtracted from the measurements of all $PM_{2.5}$ samples. The methods for calculating the parameters, including light absorption coefficients ($Abs_{365}$) and mass absorption efficiency ($MAE_{365}$) of DOM at 365 nm, as well as the absorption Ångström exponent (AAE), are presented in Text S2.

### 2.3 Isotope Analysis.

Each $PM_{2.5}$ sample was folded and placed into a 75 × 50-mm plastic box, and the $^7Be$ and $^{210}Pb$ levels were analyzed using a high-purity γ spectrometer. $^7Be$ and $^{210}Pb$ were qualitatively and quantitatively analyzed based on characteristic γ-rays. These samples were analyzed at Shenzhen University, and details of the instrument and calibrations were reported in a recent study[*Liu et al.*, 2020].

Extracts with appropriate carbon contents were spiked into clean tin cups, evaporated under gentle nitrogen flow (20–40 min), and then crushed into a ball for the analysis of carbon isotopic composition. Carbon contents of 30–50 μg and > 200 μg were used for analysis of stable and radiocarbon isotopes ($\delta^{13}C$ and $\Delta^{14}C$), respectively. The analytical procedure and instruments were described in a previous study[*Mo et al.*, 2018]. Notably, the analytical error for

stable carbon isotope ratios was within 0.2‰ (the relative standard deviation was less than 1%). $^{14}C$ analysis was carried out at the State Key Laboratory of Organic Geochemistry of GIG[*Zhu et al.*, 2015]. The $^{14}C$ values obtained were expressed as fractions of modern carbon ($f_m$) and converted into fractions of non-fossil carbon ($f_{nf}$) using the correction factor 1.052 ± 0.013 based on the long-term time series of $^{14}CO_2$ at the background station[*Levin and Kromer*, 2004; *Levin et al.*, 2013]. Standards of known age were measured as replicates to determine the instrumental error, whereas the uncertainty of $f_m$ for DOM was obtained through error propagation that included uncertainties in the DOM concentration, the variability of the reference $f_m$, and the measurement uncertainty of $f_{m,DOM}$blanks.

2.4 PMF and MLR Analyses.

The EPA5.0 PMF receptor model was used here to determine the sources of DOM. The non-fossil and fossil fractions of DOM, $DOM_{nf}$ and $DOM_{ff}$, which were calculated from the $^{14}C$ results, were added to the PMF model as primary constraints to obtain a reasonable solution. Details of the PMF method, data preparation and selection are provided in Text S3. As the PMF model generally requires a large dataset and may produce large uncertainties[*Li et al.*, 2020; *Zong et al.*, 2016], a $^{14}C$ result constrained PMF model was applied here, as $^{14}C$ analysis can quantitatively differentiate fossil and non-fossil sources of OC[*Wang et al.*, 2017b]. In this study, the combination of bootstrapping and displacement techniques, Q values (Figure S2), scaled residuals and source profiles, as well as the high match rate (≥ 80%) between bootstrapping and base case factors, a five-factor solution was chosen finally due to the interpretability of these factor profiles (Table S6). During the constraint procedure, fossil fuel-derived DOM ($DOM_{ff}$) in the BB factor was set to zero, and non-fossil DOM ($DOM_{nf}$) was set to zero for the FF factor. Additional constraint types, such as the pull-up and pull-down constraints included in the model, were also used for $DOM_{nf}$ and $DOM_{ff}$ in the secondary factors. Using this constraining method, our results showed that the relative error of predicted $f_{nf}$ to measured $f_{nf}$ for most samples was below 40% (Figure S4; calculation method discussed in Text S3). The five-factor solution obtained from the constrained run was used to represent source apportionment outcomes in the following discussion.

Considering that the measured light-absorption coefficient, $Abs_{i,j}$ [$i$, sample date; $j$, wavelength ($Mm^{-1}$)], can be expressed as the time series of mass concentrations for each factor, $F_{i,k}$ [$k$, factor number ($\mu g \cdot m^{-3}$)], we multiplied each factor with its time series of mass absorption efficiency [$MAE_{k,j}$ ($m^2 \cdot g^{-1}$ C)] (Eq. 1).

$$\mathbf{Abs}_{i,j} = \mathbf{F}_{i,k} \cdot \mathbf{MAE}_{k,j} + \boldsymbol{e}_{ij} \quad (1)$$

In this study, multivariate linear regression was used to estimate the impacts of specific DOM sources on light-absorption properties ($j$ = 365 nm)[*Geng et al.*, 2020; *Qin et al.*, 2018; *Washenfelder et al.*, 2015]. Light-absorption properties were treated as the dependent variables, and sources were independent variables. Data analysis was performed using SPSS version 21 (IBM Corporation) with the backward elimination approach. A $t$-test was used to assess the significance of the impact of each source in the model on the estimation of light-absorption properties.

2.5 Air Trajectory Generation.

As shown in Figure 1 and Table S1, 7-day backward trajectories were generated using the Hybrid Single Particle Lagrangian Integrated Trajectory (HYSPLIT) model

(https://www.ready.noaa.gov/HYSPLIT.php). Meteorological data was download from ftp://arlftp.arlhq.noaa.gov/pub/archives/. Trajectories were calculated for air masses starting from the sampling site at 500 m above ground level with 6-h intervals during the 24-h sampling period. Then, all trajectories were classified into four clusters according to the origins of the air masses and their transport pathways using the cluster calculation function in the software, including marine-origin air masses (summer monsoon period) from the Western Pacific and South East Asia regions, and continental-origin air masses (winter monsoon period) from Mongolia and Central Asia.

**Figure 1.** The location of the sampling site (Guangzhou) in this study. The backward trajectory types were clustered into four types based on their original places, including Southeast Asia (SEA), West Pacific (WP), Mongolia (MG) and Central Asia (CA) with occurrence percentage of trajectories ending at the sampling site during the entire sampling period are denoted, as described in the text. The classification for clustered air mass origins by data and season is shown in Table S1. The map was drawn using ArcGIS software, and the base map is the National Geographic Style Map from ESRI

(http://www.arcgis.com/home/webmap/viewer.html?webmap=8e75aab506924d0cbf6266268135aa80).

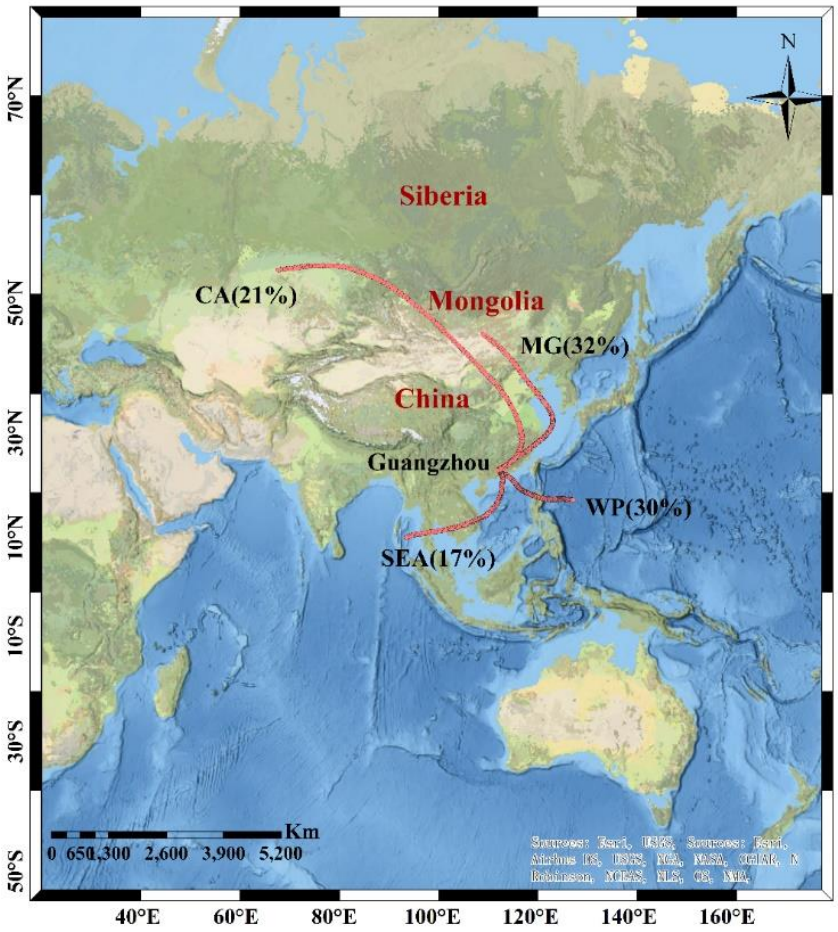


## 3 Results and Discussion

### 3.1 Temporal Variations of DOM's Light-absorption Properties.

The annual mean concentration of DOM in GZ is 5.46 ± 3.07 μg C·m$^{-3}$ (Table S2). Radiocarbon isotope analysis showed that, on average, 51 ± 8% of DOM originated from non-fossil sources. The annual average values of $Abs_{365}$, $MAE_{365}$, and AAE were 5.4 ± 4.0 M·m$^{-1}$, 0.95 ± 0.33 m$^2$·g$^{-1}$ C, and 5.7 ± 0.5, respectively. Notably, the definition of DOM used here is the same as that used for the methanol-extracted fraction, which is considered a better estimator of BrC than water-soluble organic carbon alone. Table S3 provides comparison of the light-absorption properties of DOM in this study with those obtained from methanol extracts in recent studies conducted in other parts of the world. The $Abs_{365}$ and $MAE_{365}$ values in this study are lower than those in places with poor air quality, such as Beijing[*Cheng et al.*, 2016; *Yan et al.*, 2017] and Xi'an[*Huang et al.*, 2018; *Shen et al.*, 2017b] in northern China, but higher than those in relatively clean places, such as the southeastern United States[*Liu et al.*, 2013; *Xie et al.*, 2019b] and plateau regions[*Wu et al.*, 2019; *Zhu et al.*, 2018]. The AAE values was in the range associated with laboratory generated SOA (5.2–8.8, including both biogenic and anthropogenic

SOA)[*Jiang et al.*, 2019; *Lambe et al.*, 2013; *Yan et al.*, 2016] and were comparable to those of methanol-extracted fractions measured in the southeastern United States (4.2 to 5.5 ± 0.9),[*Liu et al.*, 2013; *Xie et al.*, 2019a] but lower than those of methanol-extracted fractions from open BB emissions (6.0 ± 0.2 to 7.8 ± 3.2)[*Cheng et al.*, 2016; *Cheng et al.*, 2017; *Huang et al.*, 2018; *Shen et al.*, 2017b; *Yan et al.*, 2017] and fresh-emitted aerosols (6.29 ± 2.25 to 10.18 ± 1.27)[*Chen and Bond*, 2010; *Li et al.*, 2018; *Xie et al.*, 2017b; *Yan et al.*, 2017].

Figure 2a shows the annual variations of the light-absorption properties (including $Abs_{365}$, $MAE_{365}$, and AAE) and carbon contents of DOM. The annual trend of DOM carbon content matched well with those of $Abs_{365}$ and $MAE_{365}$, exhibiting clear seasonal variations, with enhanced values in fall and winter (November to February) and lower values in spring and summer, indicating that the carbon content and chemical composition of DOM are likely driving factors of BrC absorption. The seasonal changes in DOM content and light absorption are mainly affected by emission source, atmospheric oxidation, and air mass origin. GZ is located in the East Asian monsoon region, where north and northeast winds prevail during the winter monsoon, while southeast and southwest winds prevail during the summer monsoon. In the winter monsoon period, when $Abs_{365}$ and $MAE_{365}$ have higher values, backward trajectory analysis showed that the air masses mainly originated from the Asian continent and enter GZ through the eastern and northern parts of Guangdong province (Figure 1). During this period, the concentrations of ΣSH (hopanes and steranes) and levoglucosan, which are biomarkers of primary FF and BB, respectively, showed significant increases, indicating that the increase in DOM content and BrC absorption are likely associated with elevated levels of primary FF- and BB-origin pollutants. Notably, our $^{14}C$ results indicated that the fraction of non-fossil DOM reached its maximum (69%) although the concentrations of both fossil and non-fossil DOM increased significantly in winter. Partial correlation analysis indicated that $Abs_{365}$ had a non-significant association with fossil-derived DOM during winter, indicating that FF likely has little influence on the variations of BrC absorption. Similarly, $MAE_{365}$ was significantly related to levoglucosan ($r^2 = 0.44$, $p < 0.01$), but not significantly related to ΣSH ($p < 0.05$). In China, open straw burning during the harvest season and domestic combustion of fuels for heating during winter are widespread. Air masses transported to GZ in the harvest season and winter have passed through areas with intense BB according to fire counts (Figure S1). In those seasons, the $MAE_{365}$ values generally exceeded 1.0 $m^2 \cdot g^{-1}$ C and the highest values reached 1.94 $m^2 \cdot g^{-1}$ C, which is comparable to bulk methanol extracts from sites influenced by BB, such as Beijing (1.24 ± 0.24 to 1.46 ± 0.24 $m^2 \cdot g^{-1}$ C)[*Cheng et al.*, 2016; *Cheng et al.*, 2017; *Yan et al.*, 2017], Xi'an (1.33 ± 0.34 $m^2 \cdot g^{-1}$ C)[*Huang et al.*, 2018; *Shen et al.*, 2017a], and Seoul (1.02–1.18 $m^2 \cdot g^{-1}$ C)[*Kim et al.*, 2016]. Together, these results indicate that the increases in BrC absorption and light absorption capacity in fall and winter are mainly related to elevated BBOA.

During spring and summer (May to September), relatively low $Abs_{365}$ and $MAE_{365}$ levels were observed in GZ. The air masses transported to GZ during those seasons had passed over the South China Sea or the Western Pacific, and carried relatively clean air. At this time, FF sources, such as vehicle emissions and coal combustion, may be the primary local emission source of DOM[*Dai et al.*, 2015]. Furthermore, SOA form easily during the summer monsoon period due to high temperature and relative humidity, strong sunlight, high atmospheric oxidation levels, and high VOC emissions[*Ding et al.*, 2012]. The $MAE_{365}$ values (generally less than 1.0 $m^2 \cdot g^{-1}$ C) at this time were similar to those of vehicle emissions and laboratory-generated SOA (Table S7), indicating the possible influences of vehicle emissions and biogenic SOA formation on BrC during summer because of the high biogenic emissions and high contribution of vehicle

emissions to $PM_{2.5}$ in Guangzhou[*Dai et al.*, 2015]. We found that the seasonal changes in the contribution of fossil emissions to DOM was non-significant, while relatively low BB emissions occurred in spring and summer; these findings were supported by the similar ΣSH/DOM ratios for the winter and summer monsoon periods ($0.5 \pm 0.3$ vs. $0.6 \pm 0.2$ ng·μg$^{-1}$ C). Meanwhile, a marked decrease was observed in the levoglucosan/DOM ratio from $10.07 \pm 6.8$ ng·μg$^{-1}$ C during the winter monsoon to $5.1 \pm 3.1$ ng·μg$^{-1}$ C in the summer monsoon, suggesting that the lower $MAE_{365}$ values of the summer monsoon period are likely related to low BB emissions, and the source of BrC probably could be attributed to FF. Moreover, high concentrations of biogenic tracers, namely isoprene- and monoterpene-derived SOA, were also observed during the summer monsoon period (Figure 2b). Generally, BrC generated from biogenic precursors has a lower absorption capacity than that generated from BB. Therefore, our results indicate that the relatively low BrC absorption at GZ during the summer monsoon period may be related to the high levels of biogenic SOA processes.

**Figure 2**. (a) Temporal variations in (a) light absorption properties ($Abs_{365}$, $MAE_{365}$ and AAE) and carbon contents of DOM, mass concentrations of (b) biogenic SOA tracers (B-SOA), levoglucosan (levo) and sum of steranes and hopanes (ΣSH). The biogenic SOA tracers (B-SOA) include isoprene- (MTLs: sum of 2-Methylthreitol and 2-Methylerythritol) and monoterpene-derived SOA (Mono-SOA: sum of 3-Hydorxyglutaric, 3-Methyl-1,2,3-butanetricarboxylic acid, cis-Pinonic acid).

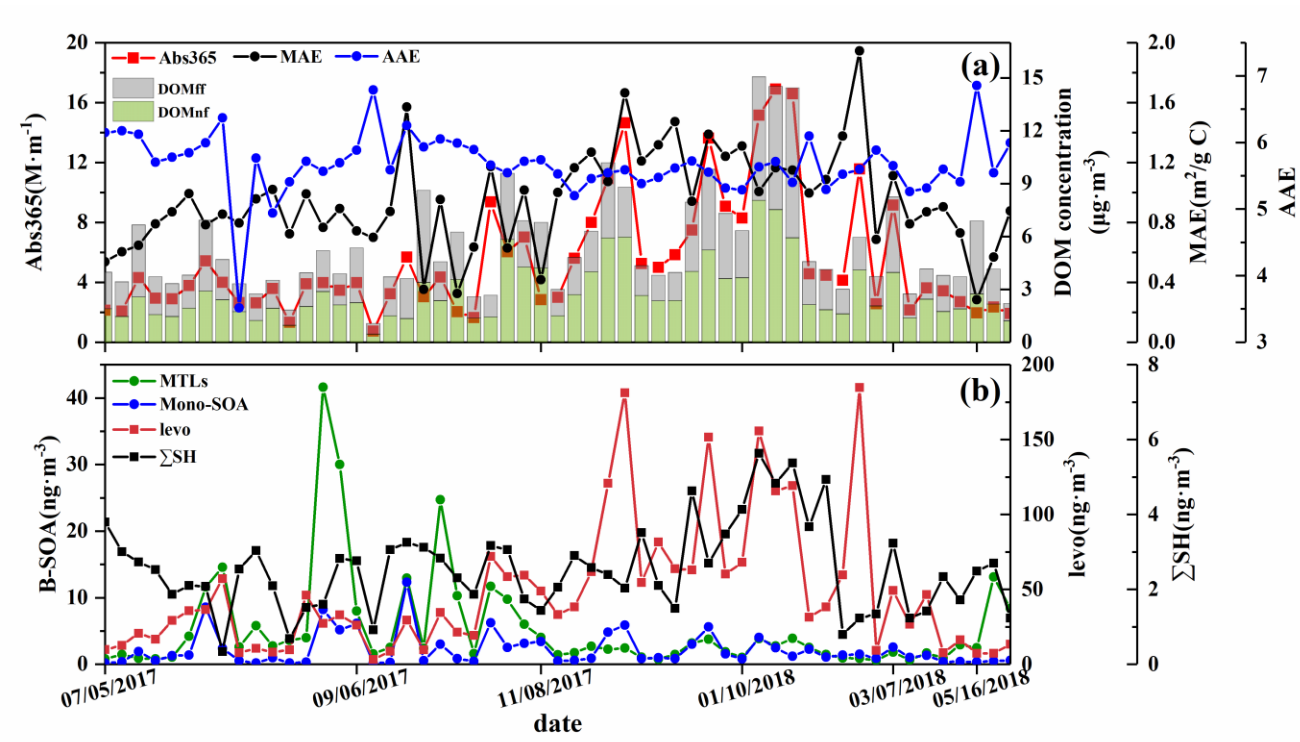


3.2 Sources apportionment of DOM.

To further quantitatively determine the sources of DOM and BrC, we applied a $^{14}C$-constrained PMF model. Using $^{14}C$ results as a constraint can reduce the uncertainty (over- or underestimation) arising from PMF source apportionment[*Li et al.*, 2020; *Zong et al.*, 2016].

Figure S3 shows the factor profile and time series of factor contributions to DOM for the five-factor solution obtained using the $^{14}C$-constrained PMF model, which includes two primary factors, BB and FF, as well as three factors (NT, PW-SOA, and ISO+OS, defined as follows) associated with secondary processes. NT represents high loading of nitrates and ammonium, which should be associated with secondary nitrate formation. PW-SOA is associated with the combination of SOA formation from photochemical processes and waste combustion, as SMG acids (sum of succinic acid, malic acid and glutaric acid), *o-/m*-phthalic acid, and monoterpene SOA can be products of photochemical processes, and *p*-phthalic acid is an indicator of waste combustion, especially plastic combustion[*Kawamura and Pavuluri*, 2010]. ISO+OS has high loadings of isoprene-derived SOA, $SO_4^{2-}$ and fatty acids, and thus may be classified as a mixed factor of isoprene-derived SOA and organic sulfates. As shown in Figures 3a & S3, the highest average contribution to DOM was from the primary factor FF, which was responsible for 32% of total DOM and showed small changes in concentration across the year, suggesting relatively stable emissions from FF sources. This result is reasonable, as GZ is one of the largest cities in China, vehicle emissions and industrial coal combustion are important sources of air pollution, which could account for >50% of total $PM_{2.5}$ (http://www.gz.gov.cn/xw/zwlb/bmdt/ssthjj/content/post_5516998.html). BB explained 18% of the DOM and showed a marked increasing trend from fall to winter, consistent with other studies of OC apportionment in this region[*Huang et al.*, 2014; *Wang et al.*, 2015]. In total, SOA factors were responsible for 50% of DOM mass, most of which was contributed by NT (20%) and ISO+OS (22%), while PW-SOA only accounted for 7% of DOM. DOM formed from NT showed higher concentrations in fall and winter, while the opposite pattern was observed for DOM formed from ISO+OS, which had lower concentrations in winter than in other seasons. Our results are comparable to those reported in previous studies, which found that secondary OC comprised a large fraction of OC in the Pearl River Delta region[*Huang et al.*, 2014; *Qin et al.*, 2017; *Wang et al.*, 2017a], highlighting the importance of SOA to atmospheric organic matter. We noted that the secondary factors were also assigned to fossil and non-fossil fractions based on the built-in multilinear engine used by PMF[*Norris et al.*, 2014]. Therefore, we calculated the contents of fossil and non-fossil secondary DOM, and the calculation method is presented in Text S3. As shown in Figure 3b & c, our results further indicate that secondary DOM in GZ was dominated by non-fossil carbon, with an average 69 ± 8% of secondary DOM, comparable with previous works[*Huang et al.*, 2014; *Zhang et al.*, 2018]. Notably, the content of non-fossil DOM obtained from our $^{14}C$-constrained PMF model had a strong correlation with the measured values ($r = 0.86$, $p < 0.01$, Figure S4a & b), showing an average relative error of less than 40%. In general, our results show that the $^{14}C$-constrained PMF model can relatively accurately

determine the sources of atmospheric DOM, providing a strong foundation for BrC source apportionment.

**Figure 3**. Average contribution of each factors to the (a) DOM and (b) secondary DOM. (c) The time-series of non-fossil fraction of secondary DOM. Calculation methods are presented in Text S3 in the Supporting Information. The "nf" and "ff" denote non-fossil and fossil fuels fractions.

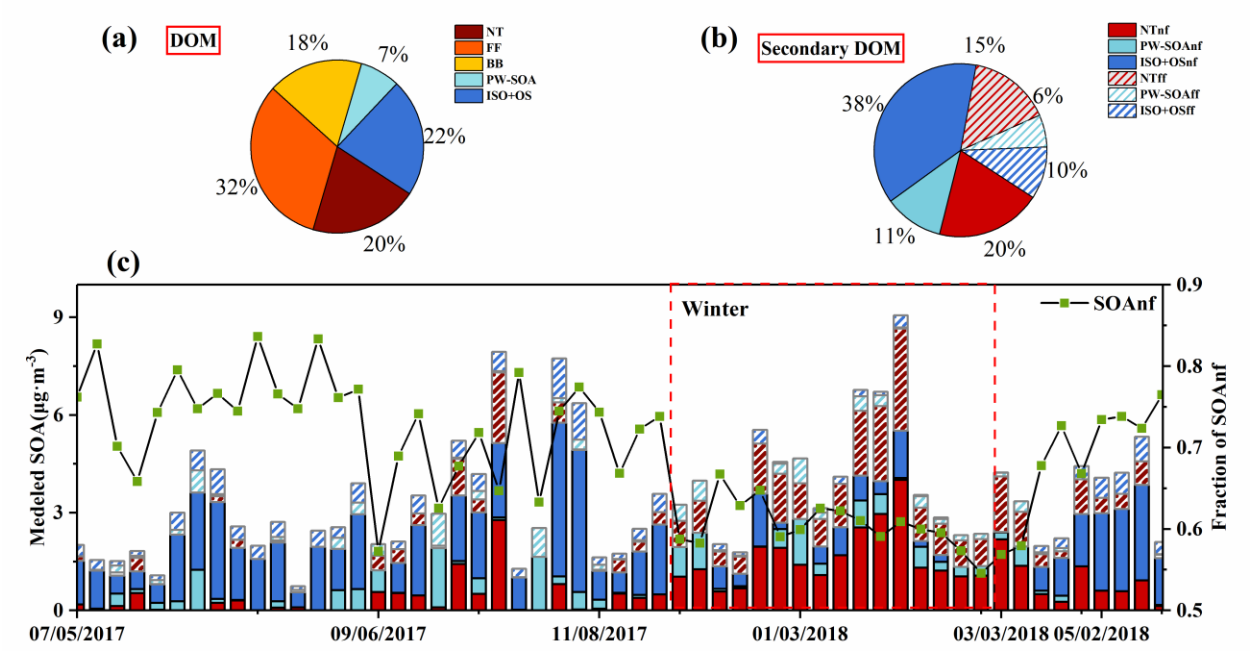


3.3 Possible Source Contributions to BrC Adsorption.

Although several studies have characterized BrC absorption properties in GZ, the detailed source contributions to BrC absorption remain unclear[*Liu et al.*, 2018; *Qin et al.*, 2018]. To determine the specific source contributions to BrC absorption, we further employed MLR analysis to assign BrC absorption to the five factors obtained from PMF (BB, FF, NT, PW-SOA, and ISO+OS), as shown in Equation 2[*Geng et al.*, 2020]. For BrC formed through secondary processes, we only considered the formation pathways, regardless of the fossil or non-fossil source of its precursor, as a given formation pathway may usually generates secondary BrC with similar structures or functional groups.

$$\mathbf{Abs}_{365} = a\,C_{NT} + b\,C_{FF} + c\,C_{BB} + d\,C_{PW\text{-}SOA} + e\,C_{ISO+OS}, \quad (2)$$

where the coefficients *a*, *b*, *c*, *d*, and *e* represent the MAE of each factor ($m^2 \cdot g\ C^{-1}$) and $C_{NT}$, $C_{FF}$, $C_{BB}$, $C_{PW\text{-}SOA}$, and $C_{ISO+OS}$ represent the mass concentration of each factor. The final model is reasonable (N = 55) with an *r* of 0.97 and mean error between predicted and measured $Abs_{365}$ of 17% (Figure S4c & d). The modeled $MAE_{365}$ values for each factor are presented in Table S7 and our results align well with those reported from previous laboratory experiments and field studies. However, $MAE_{365}$ values obtained from the regression model have uncertainties arising from measurement error, interpolation of data, source apportionment, or possibly from incomplete source information in the PMF model[*Bates et al.*, 2015].

Figure 4a shows the time series of BrC absorption for factors 1–5 and their mean contributions to the total modeled $Abs_{365}$. The primary emission factor of FF accounted for the highest average proportion (33.7%) of total BrC absorption in this study. Due to the relatively large and stable FF emissions from vehicles and power plants throughout the year, FF is the main contributor to BrC in GZ. To date, few studies have reported the contribution of FF to BrC in the atmosphere. Our results show that although DOM from BB accounts for only 18% of total DOM by mass, it contributes 27.3% of total $Abs_{365}$, in accordance with the findings of a previous study conducted in GZ (26% at 370 nm)[*Qin et al.*, 2018]. The ratio in GZ is lower than those in BB-influenced areas, such as Beijing (58%)[*Du et al.*, 2014], Atlanta (50%)[*Hecobian et al.*, 2010], and Alabama (87%)[*Washenfelder et al.*, 2015], but higher than that in a less-polluted region of North Carolina (14%)[*Xie et al.*, 2019b]. Furthermore, we found that the proportion of SOA-sourced BrC absorption in this study (39%) was in the same range as values in Xi'an ($\lambda$ = 370 nm, 19–48%), but much lower than those recorded on the Tibetan Plateau (70%) and Hong Kong (76%)[*Wang et al.*, 2019a; *Wang et al.*, 2019b; *Zhang et al.*, 2020], highlighting the importance of secondary sources to BrC formation in GZ. Among secondary sources, NT is the most important source of secondary BrC, accounting for 16.4% of total BrC absorption. Although ISO+OS was responsible for a relatively large fraction of DOM mass, the BrC formed through this secondary process only accounted for an average of about 9% of total BrC absorption, likely due to the weak light-absorbing capacity of biogenic SOA.

The seasonal trends of BrC absorption attributed to the five sources are similar to those of their DOM. BrC absorption associated with FF was relatively stable throughout the year, while BB and NT showed increases in contributions to BrC absorption during the winter monsoon period. Backward trajectory analysis showed that continental air masses were dominant in the winter monsoon period (Figure 1 and Table S1). As shown in Figure 4b, the absorption contribution of BB varied markedly among trajectory clusters and was dominant in continental-origin air masses from Mongolia and Central Asia, which had levels 3–4 times than those of marine-origin air masses. This finding indicates a possible influence from continental BBOA transport during winter when BrC is elevated, which is consistent with previous studies that identified the main driver of air pollution in GZ as allochthonous inputs[*Andreae et al.*, 2008; *Liu et al.*, 2014].

**Figure 4**. (a)The time-series of $Abs_{365}$ contributed by each factor. The pie chart shows the average contribution of each factor to the light absorption. (b) The relative contribution of each factor to the total BrC absorption for the different air masses clusters. The four backward

trajectory clusters include Southeast Asia (SEA), West Pacific (WP), Mongolia (MG) and Central Asia (CA).

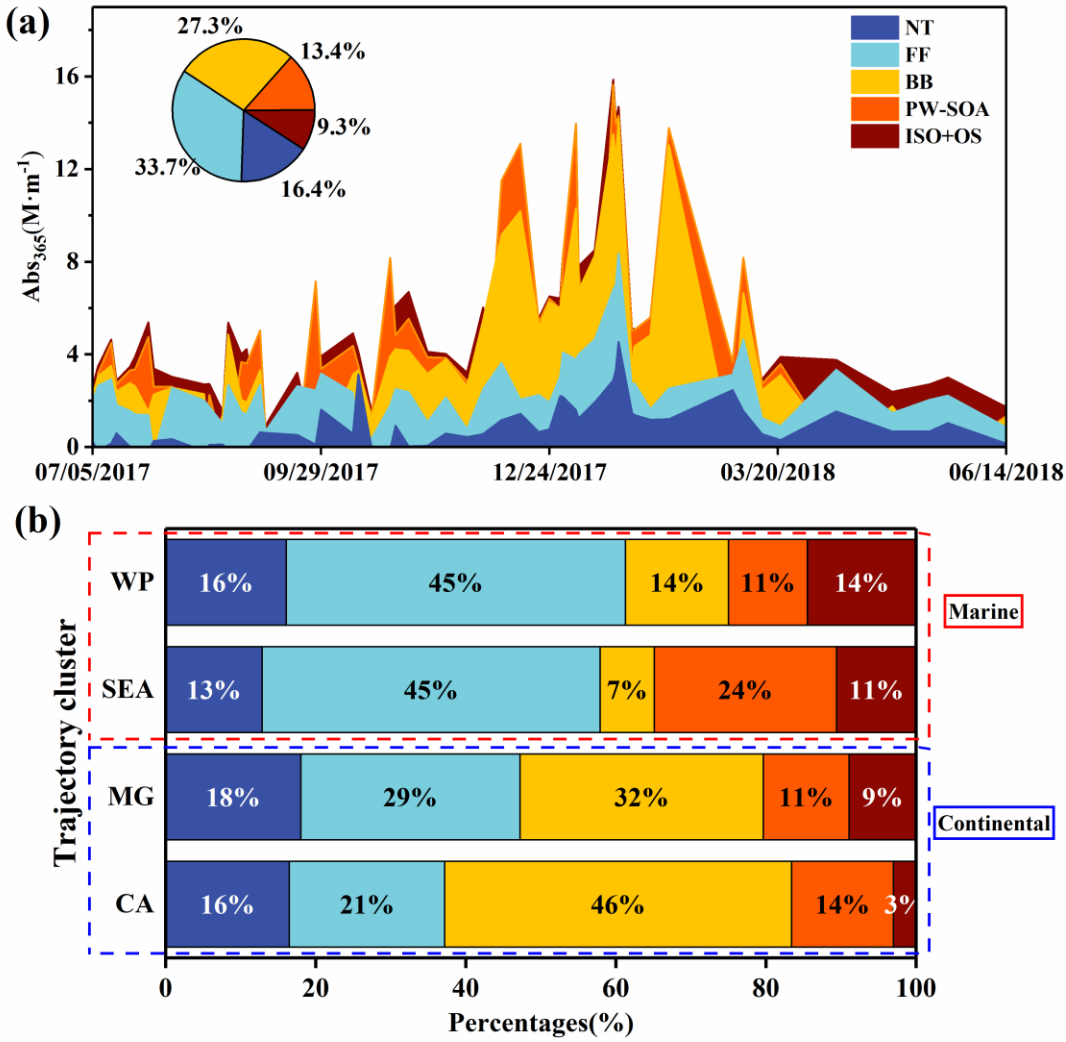


3.4 Characterize the BrC Transport Processes with $^{210}$Pb and $^{7}$Be.

As described above, enhanced atmospheric BrC absorption in GZ during the winter monsoon period could be largely due to allochthonous inputs. $^{210}$Pb is one of the most effective indicators for characterizing the transport of submicron aerosols from continents, which can be used to estimate the influence of terrestrial aerosol transport on receptor sites. Overall, the annual variations of $^{210}$Pb indicated that their concentrations increased from fall to winter and then decreased in spring (Figure 5), consistent with the variations in $Abs_{365}$ observed during the sampling campaign. The average activity concentration of $^{210}$Pb on days influenced by continental air masses was double that on days affected by marine air masses (Table S4). Notably, the decreased planetary boundary layer height (PBLH) in fall and winter may lead to misjudgment of the input of allochthonous particles. A previous study reported that $^{210}$Pb is relatively insensitive to short-term variations in PBLH[*Hammer et al.*, 2007]. In this study, as shown in Figure S5, the PBLH showed characteristic low levels in fall and winter and high levels in spring and summer. Regardless of changes in PBLH, the activity of $^{210}$Pb was relatively

constant in spring and summer; meanwhile, in fall and winter, the PBLH was relatively stable but the activity concentration of $^{210}$Pb varied widely. Moreover, the ratios of $^{210}$Pb to $PM_{2.5}$ were also higher during the winter monsoon season ($0.05 \pm 0.02$ mBq·μg$^{-1}$) than the summer monsoon season ($0.03 \pm 0.02$ mBq·μg$^{-1}$). These results support the role of allochthonous inputs as one of the main drivers of the increase in atmospheric particulate matter and BrC absorption during the winter monsoon period in GZ.

During the prevailing winter monsoon season, we observed positive correlations of the concentration of $^{210}$Pb with measured $Abs_{365}$ ($r = 0.68$, $p < 0.01$), non-fossil DOM ($r = 0.71$, $p < 0.01$), and the concentration of levoglucosan ($r = 0.64$, $p < 0.01$, Figure S6), confirming that the main reason for the increase in BrC absorption in GZ during the winter monsoon is likely related to allochthonous inputs of BBOA. In contrast, during the summer monsoon season, no significant correlation was found between $^{210}$Pb and $Abs_{365}$ ($r = 0.39$, $p > 0.05$), indicating that BrC mainly originates from local primary and secondary sources.

However, we noted that high $^{210}$Pb was not always accompanied by high BrC absorption (Figure 5). For example, high $^{210}$Pb in conjunction with low $Abs_{365}$ and low $DOM_{nf}$ was observed on December 28, 2017 (point A). In this case, $^{7}$Be, a useful indicator for characterizing the upper atmosphere and surface exchange processes, was high. Backward trajectory analysis showed that a strong cold Siberian air mass intruded into China and sank in South China due to high wind speed. This probably suggests that invading Siberian air masses carry less pollution, which leads to dilution and diffusion of local pollutants, resulting in decreases in the particle concentration and BrC absorption. Considering that transport processes include ground-level transport and long-range processes in the upper atmosphere, we introduced the index of $f(^{7}\mathrm{Be}, ^{210}\mathrm{Pb})$, which combines $^{7}$Be and $^{210}$Pb to reveal the effects of atmospheric transport on variations in light absorption. The $f(^{7}\mathrm{Be}, ^{210}\mathrm{Pb})$ index was defined as follows in a previous study[*Graustein and Turekian*, 1996]:

$$f\left(^{7}\mathrm{Be}, ^{210}\mathrm{Pb}\right) = \frac{[^{7}\mathrm{Be}]}{[^{7}\mathrm{Be}]+n[^{210}\mathrm{Pb}]} \quad (3)$$

where $[^{7}\mathrm{Be}]$ and $[^{210}\mathrm{Pb}]$ denote the activity concentrations of the corresponding nuclides, and $n$ is approximated by the ratio of the standard deviation of $^{7}$Be to the standard deviation of $^{210}$Pb. Notably, $f(^{7}\mathrm{Be}, ^{210}\mathrm{Pb})$ avoids the influence of precipitation scavenging and provides a useful tool for clearly understanding the dynamic transport of BrC. Air masses with low $f(^{7}\mathrm{Be}, ^{210}\mathrm{Pb})$ represent continental surface emission sources, whereas high $f(^{7}\mathrm{Be}, ^{210}\mathrm{Pb})$ values are associated with sources in the upper atmosphere[*Grossi et al.*, 2016; *Lin et al.*, 2014]. During the winter monsoon period, the trend of BrC absorption was the inverse of that of $f(^{7}\mathrm{Be}, ^{210}\mathrm{Pb})$, especially during period II, as shown in Figure 5. We found that the concentration of $DOM_{nf}$ and BrC absorption generally decreased about 1–2 times and 2–3 times, respectively, for high-altitude transport (high $f(^{7}\mathrm{Be}, ^{210}\mathrm{Pb})$) relative to near-surface transport (low $f(^{7}\mathrm{Be}, ^{210}\mathrm{Pb})$). Two samples that exemplify this trend are denoted in Figure 5 and S7. These analyses were conducted for the aerosol samples collected on January 3 (point B) and 10 (point C), which correspond to surface transport (for at least 72 h, low $f(^{7}\mathrm{Be}, ^{210}\mathrm{Pb})$ and high $Abs_{365}$) and direct downdrafting of the upper atmosphere after long-distance transport from the north (high $f(^{7}\mathrm{Be}, ^{210}\mathrm{Pb})$ and low $Abs_{365}$), respectively. Although the BrC absorption of aerosols collected on January 10 was markedly lower than that of samples collected on January 3, the $MAE_{365}$ of DOM showed little change (1.31 m$^2$·g$^{-1}$ C vs. 1.39 m$^2$·g$^{-1}$ C). Generally, $MAE_{365}$ decreases significantly during long-range transport due to photochemical degradation effects[*Dasari et al.*, 2019; *Zheng et al.*,

2020]. Therefore, BrC transported at high altitude should have higher $MAE_{365}$ values in the initial source region. Compared with the samples collected on January 3, 2018, the aerosols from January 10, 2018, had a lower fossil fuel ratio (0.47 vs. 0.43) but a higher concentration of ΣSH (about 2.3 times), indicating that the important influence of primary source of FF. Although the oxidative aging of particulate levoglucosan occurs during the long-range transport process[*Gensch et al.*, 2018], the elevated non-fossil ratio and levoglucosan level also indicate the importance of BB. Notably, primary emissions of BB and FF are typically high in aerosols during the heating period in northern China[*Yan et al.*, 2018], where the $MAE_{365}$ values of methanol extracts were 1.45 ± 0.26 $m^2 \cdot g^{-1}$ C (maximum: 2.07 $m^2 \cdot g^{-1}$ C). Accordingly, our results indicate that $MAE_{365}$ values may be reduced by 10% or even more due to the effects of photochemical bleaching during upper-atmosphere transport processes.

**Figure 5**. Annual variability trends of $^{7}Be$ and $^{210}Pb$ at GZ. The insert shows the variations of $^{7}Be/^{210}Pb$ ratios and the $Abs_{365}$ during the period II which from Nov.8, 2017 to Jan. 25, 2018 at GZ. The point A, B and C are marked by pink frame are typical examples. We again presented the BrC absorption and the mass concentration of non-fossil-derived DOM for better comparison with the two natural radionuclide tracers of $^{7}Be$ and $^{210}Pb$.

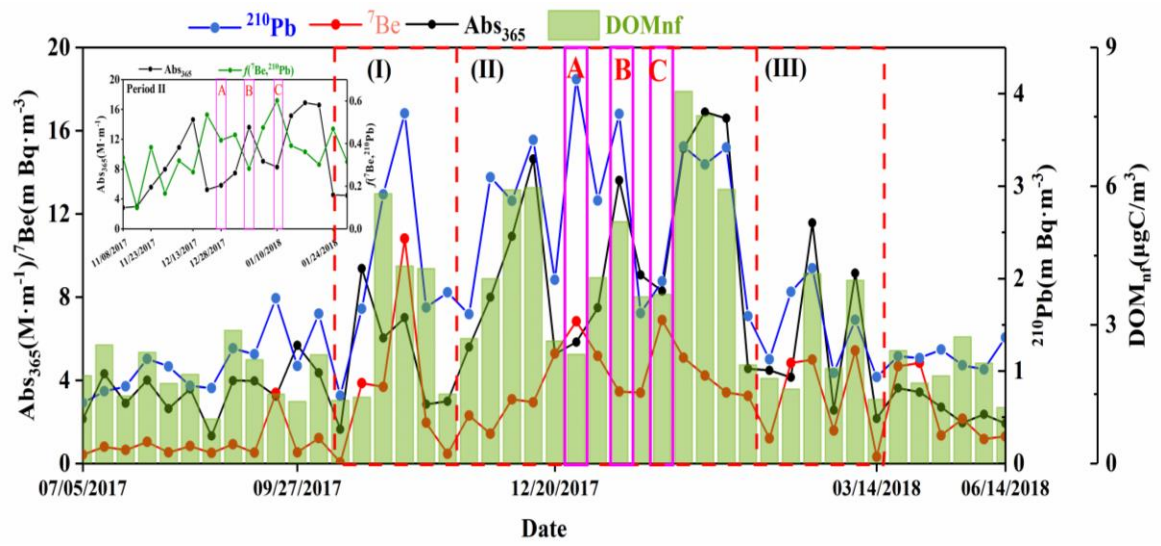


### 3.5 $^{210}Pb$-based Estimation of the Contribution of Atmospheric Transport to BrC Absorption.

Given that the background value of $^{210}Pb$ in GZ is difficult to determine, we used the average activity concentration of $^{210}Pb$ on days influenced by marine air masses as the background value. The average activity concentration of $^{210}Pb$ in the marine air masses was 1.03 ± 0.23 $mBq \cdot m^{-3}$. We set criteria that an activity concentration of $^{210}Pb$ higher than 1.03 $mBq \cdot m^{-3}$ indicated the influence of transported aerosols, while lower values reflected only local emission sources. Thus, BrC absorption due to local emissions sources ($Abs_{365(local)}$) during the winter monsoon period was estimated as 3.65 $M \cdot m^{-1}$ based on the linear correlation between measured $Abs_{365}$ and $^{210}Pb$ ($y = 3.15x + 0.40$) determined using the set background value of $^{210}Pb$. The impact of arriving air masses on the local atmospheric environment not only causes overlay of their components, but also chemical reactions among them. Therefore, we hypothesized that the measured $Abs_{365}$ value was representative of the sum of local and transported BrC (i.e.,

reaggregation on local particles), neglecting the impact of newly generated BrC, such as secondary BrC formation from transported VOCs. And the transported BrC can be calculated by subtracting the $Abs_{365(local)}$:

$$Abs_{365(transport)} = Abs_{365} - Abs_{365(local)} \quad (4)$$

Figure S8 shows the estimated transported fraction of BrC absorption during the winter monsoon season. Note that negative values likely resulted from dilution effects, as low $DOM_{nf}$ was observed. The mean value on days of elevated BrC was 49 ± 23% (excluding negative values), showing that half of BrC absorption is associated with transport aerosols. Combined with the results of PMF analysis, the variations of $^{210}Pb$ on days influenced by continental air masses were positively correlated with BrC absorption from BB and NT sources ($p < 0.01$), suggesting the transport aerosols were mainly associated with BBOA and secondary nitrates[*Yu et al.*, 2020]. However, we also found that BrC absorption from BB was about 2–3 times that from NT sources, indicating that invasive BrC was mainly contributed by primary emissions of BB. Although transport processes were influenced by complex meteorological parameters such as wind direction and speed, our very rough estimate highlights the importance of long-range BBOA transport to BrC absorption at the regional scale. And more researches in accurately assessing the contribution of regional transport aerosols to BrC absorption or radiative forcing are needed in the future.

## 4 Conclusions

In this study, $PM_{2.5}$ samples were collected at Guangzhou, a big city where under the influence of oceanic subtropical monsoon climate. The sources of atmospheric dissolved organic matters and soluble BrC in $PM_{2.5}$, and the key factors influencing BrC's seasonality were explore. Our results show that the primary sources of fossil-fuel combustion and biomass burning contributed 32% and 18% of DOM at Guangzhou, respectively; the secondary process could account for 50% of DOM, with 69% of them were non-fossil carbon.We found that the BrC absorption increased substantially during winter monsoon, while decreased dring summer monsoon. Correspondingly, the contributions of biomass burning and secondary nitrates formation to BrC absorption increased and dominant during winter monsoon, and fossil-fuel combustion and biogenic organosulfates formation were the main contributors of BrC (Figure 4) during summer monsoon. Furthermore, in keeping with $Abs_{365}$, levoglucosan and $NO_3^-$, the acitivity concentration of $^{7}Be$ and $^{210}Pb$ also largely increased during winter monsoon, indicating the significance of regional transportation of biomass burning organic aerosols and related secondary nitrates formation processes on BrC absorption enhancement.

From the regional and global scale, biomass burning happens frequently such as the seriously crops combustion events in the India Plain and the wildfire in the Amazon rainforest and African grass plains. All these extensive biomass burning aerosols emissions formed extensive atmospheric brown clouds and will transported form the sources regions to everywhere of the world with the air masses. The high light-absorption capacity of BrC will change the balance of radiative forcing and result to the climate abnormal changes as well as the change of hydrological cycle. Therefore, it is not only the urgent need of the source area, but also the help of international cooperation to reduce the emissions of biomass combustion in the disaster area of the world.

## Acknowledgments

This study was supported by the Natural Science Foundation of China (NSFC; Nos. 42030715 and 41773120), State Key Laboratory of Organic Geochemistry, GIGCAS (Grant No. SKLOG 2016-A05 and SKLOG 2020-05), and Guangdong Foundation for Program of Science and Technology Research (Grant No. 2017B030314057, 2019B121205006 and 2020B1212060053). The authors declare no competing financial interest. Data supporting this paper can be found in Harvard Dataverse (https://doi.org/10.7910/DVN/IHGX3X).

## References

Andreae, M. O., &Gelencsér, A. (2006), Black carbon or brown carbon? The nature of light-absorbing carbonaceous aerosols, *Atmospheric Chemistry and Physics*, *6*(10), 3131-3148, https://doi:10.5194/acp-6-3131-2006

Andreae, M. O., Schmid, O., Yang, H., Chand, D., Zhen Yu, J., Zeng, L.-M., &Zhang, Y.-H. (2008), Optical properties and chemical composition of the atmospheric aerosol in urban Guangzhou, China, *Atmospheric Environment*, *42*(25), 6335-6350, https://doi:10.1016/j.atmosenv.2008.01.030

Barrett, T. E., &Sheesley, R. J. (2017), Year-round optical properties and source characterization of Arctic organic carbon aerosols on the North Slope Alaska, *Journal of Geophysical Research: Atmospheres*, *122*(17), 9319-9331, https://doi:10.1002/2016jd026194

Bates, J. T., Weber, R. J., Abrams, J., Verma, V., Fang, T., Klein, M., et al. (2015), Reactive Oxygen Species Generation Linked to Sources of Atmospheric Particulate Matter and Cardiorespiratory Effects, *Environmental Science & Technology*, *49*(22), 13605-13612, https://doi:10.1021/acs.est.5b02967

Bikkina, S., Andersson, A., Ram, K., Sarin, M. M., Sheesley, R. J., Kirillova, E. N., et al. (2017), Carbon isotope-constrained seasonality of carbonaceous aerosol sources from an urban location (Kanpur) in the Indo-Gangetic Plain, *Journal of Geophysical Research: Atmospheres*, *122*(9), 4903-4923, https://doi:10.1002/2016jd025634

Chen, Y., &Bond, T. C. (2010), Light absorption by organic carbon from wood combustion, *Atmospheric Chemistry and Physics*, *10*(4), 1773-1787,

Cheng, Y., He, K.-b., Du, Z.-y., Engling, G., Liu, J.-m., Ma, Y.-l., et al. (2016), The characteristics of brown carbon aerosol during winter in Beijing, *Atmospheric Environment*, *127*, 355-364, https://doi:10.1016/j.atmosenv.2015.12.035

Cheng, Y., He, K. B., Engling, G., Weber, R., Liu, J. M., Du, Z. Y., &Dong, S. P. (2017), Brown and black carbon in Beijing aerosol: Implications for the effects of brown coating on light absorption by black carbon, *Science of the Total Environment*, *599-600*, 1047-1055, https://doi:10.1016/j.scitotenv.2017.05.061

Dai, S., Bi, X., Chan, L. Y., He, J., Wang, B., Wang, X., et al. (2015), Chemical and stable carbon isotopic composition of PM2.5 from on-road vehicle emissions in the PRD region and implications for vehicle emission control policy, *Atmospheric Chemistry and Physics*, *15*(6), 3097-3108, https://doi:10.5194/acp-15-3097-2015

Dasari, S., Andersson, A., Bikkina, S., Holmstrand, H., Budhavant, K., Satheesh, S., et al. (2019), Photochemical degradation affects the light absorption of water-soluble brown carbon in the South Asian outflow, *Science Advances*, *5*(1), eaau8066, https://doi:10.1126/sciadv.aau8066

Desyaterik, Y., Sun, Y., Shen, X., Lee, T., Wang, X., Wang, T., &Collett, J. L. (2013), Speciation of "brown" carbon in cloud water impacted by agricultural biomass burning in eastern China, *Journal of Geophysical Research: Atmospheres*, *118*(13), 7389-7399, https://doi:10.1002/jgrd.50561

Ding, X., Wang, X.-M., Gao, B., Fu, X.-X., He, Q.-F., Zhao, X.-Y., et al. (2012), Tracer-based estimation of secondary organic carbon in the Pearl River Delta, south China, *Journal of Geophysical Research*, *117*, D05313, https://doi:10.1029/2011JD016596

Du, Z., He, K., Cheng, Y., Duan, F., Ma, Y., Liu, J., et al. (2014), A yearlong study of water-soluble organic carbon in Beijing II: Light absorption properties, *Atmospheric Environment*, *89*, 235-241, https://doi:10.1016/j.atmosenv.2014.02.022

Geng, X., Mo, Y., Li, J., Zhong, G., Tang, J., Jiang, H., et al. (2020), Source apportionment of water-soluble brown carbon in aerosols over the northern South China Sea: Influence from land outflow, SOA formation and marine emission, *Atmospheric Environment*, *229*, https://doi:10.1016/j.atmosenv.2020.117484

Gensch, I., Sang-Arlt, X. F., Laumer, W., Chan, C. Y., Engling, G., Rudolph, J., &Kiendler-Scharr, A. (2018), Using delta(13)C of Levoglucosan As a Chemical Clock, *Environmental Science & Technology*, *52*(19), 11094-11101, https://doi:10.1021/acs.est.8b03054
Graustein, W. C., &Turekian, K. K. (1996), 7Be and210Pb Indicate an upper troposphere source for elevated ozone in the summertime subtropical free troposphere of the eastern North Atlantic, *Geophysical Research Letters*, *23*(5), 539-542, https://doi:10.1029/96gl00304
Grossi, C., Ballester, J., Serrano, I., Galmarini, S., Camacho, A., Curcoll, R., et al. (2016), Influence of long-range atmospheric transport pathways and climate teleconnection patterns on the variability of surface (210)Pb and (7)Be concentrations in southwestern Europe, *Journal of Environmental Radioactivity*, *165*, 103-114, https://doi:10.1016/j.jenvrad.2016.09.011
Gustafsson, O., Krusa, M., Zencak, Z., Sheesley, R. J., Granat, L., Engstrom, E., et al. (2009), Brown clouds over South Asia: biomass or fossil fuel combustion?, *Science*, *323*(5913), 495-498, https://doi:10.1126/science.1164857
Hammer, S., Wagenbach, D., Preunkert, S., Pio, C., Schlosser, C., &Meinhardt, F. (2007), Lead-210 observations within CARBOSOL: A diagnostic tool for assessing the spatiotemporal variability of related chemical aerosol species?, *Journal of Geophysical Research*, *112*(D23), https://doi:10.1029/2006jd008065
Healy, R. M., Wang, J. M., Jeong, C. H., Lee, A. K. Y., Willis, M. D., Jaroudi, E., et al. (2015), Light-absorbing properties of ambient black carbon and brown carbon from fossil fuel and biomass burning sources, *Journal of Geophysical Research: Atmospheres*, *120*(13), 6619-6633, https://doi:10.1002/2015jd023382
Hecobian, A., Zhang, X., Zheng, M., Frank, N., Edgerton, E. S., &Weber, R. J. (2010), Water-Soluble Organic Aerosol material and the light-absorption characteristics of aqueous extracts measured over the Southeastern United States, *Atmospheric Chemistry and Physics*, *10*(13), 5965-5977, https://doi:10.5194/acp-10-5965-2010
Huang, R. J., Yang, L., Cao, J. J., Chen, Y., Chen, Q., Li, Y., et al. (2018), Brown Carbon Aerosol in Urban Xi'an, Northwest China: The Composition and Light Absorption Properties, *Environmental Science & Technology*, *52*(12), 6825-6833, https://doi:10.1021/acs.est.8b02386
Huang, R. J., Zhang, Y., Bozzetti, C., Ho, K. F., Cao, J. J., Han, Y., et al. (2014), High secondary aerosol contribution to particulate pollution during haze events in China, *Nature*, *514*(7521), 218-222, https://doi:10.1038/nature13774
Jiang, H., Frie, A. L., Lavi, A., Chen, J. Y., Zhang, H., Bahreini, R., &Lin, Y.-H. (2019), Brown Carbon Formation from Nighttime Chemistry of Unsaturated Heterocyclic Volatile Organic Compounds, *Environmental Science & Technology Letters*, *6*(3), 184-190, https://doi:10.1021/acs.estlett.9b00017
Jiang, H., Zhong, G., Wang, J., Jiang, H., Tian, C., Li, J., et al. (2018), Using Polyurethane Foam-Based Passive Air Sampling Technique to Monitor Monosaccharides at a Regional Scale, *Environmental Science & Technology*, *52*, 12546-12555, https://doi:10.1021/acs.est.8b02254
Kawamura, K., &Pavuluri, C. M. (2010), New Directions: Need for better understanding of plastic waste burning as inferred from high abundance of terephthalic acid in South Asian aerosols, *Atmospheric Environment*, *44*(39), 5320-5321, https://doi:10.1016/j.atmosenv.2010.09.016
Kim, H., Kim, J. Y., Jin, H. C., Lee, J. Y., &Lee, S. P. (2016), Seasonal variations in the light-absorbing properties of water-soluble and insoluble organic aerosols in Seoul, Korea, *Atmospheric Environment*, *129*, 234-242, https://doi:10.1016/j.atmosenv.2016.01.042
Kirillova, E. N., Andersson, A., Han, J., Lee, M., &Gustafsson, Ö. (2014a), Sources and light absorption of water-soluble organic carbon aerosols in the outflow from northern China, *Atmospheric Chemistry and Physics*, *14*(3), 1413-1422, https://doi:10.5194/acp-14-1413-2014
Kirillova, E. N., Andersson, A., Tiwari, S., Srivastava, A. K., Bisht, D. S., &Gustafsson, Ö. (2014b), Water-soluble organic carbon aerosols during a full New Delhi winter: Isotope-based source apportionment and optical properties, *Journal of Geophysical Research: Atmospheres*, *119*(6), 3476-3485, https://doi:10.1002/2013jd020041
Lambe, A. T., Cappa, C. D., Massoli, P., Onasch, T. B., Forestieri, S. D., Martin, A. T., et al. (2013), Relationship between oxidation level and optical properties of secondary organic aerosol, *Environmental Science & Technology*, *47*(12), 6349-6357, https://doi:10.1021/es401043j
Levin, I., &Kromer, B. (2004), The Tropospheric 14CO2 Level in Mid-Latitudes of the Northern Hemisphere (1959–2003), *Radiocarbon*, *46*(3), 1261-1272, https://doi:10.1017/s0033822200033130
Levin, I., Kromer, B., &Hammer, S. (2013), Atmospheric Δ14CO2 trend in Western European background air from 2000 to 2012, *Tellus B: Chemical and Physical Meteorology*, *65*(1), https://doi:10.3402/tellusb.v65i0.20092
Li, J. J., Wang, G. H., Cao, J. J., Wang, X. M., &Zhang, R. J. (2013), Observation of biogenic secondary organic aerosols in the atmosphere of a mountain site in central China: temperature and relative humidity effects, *Atmospheric Chemistry and Physics*, *13*(22), 11535-11549, https://doi:10.5194/acp-13-11535-2013

Li, M., Fan, X., Zhu, M., Zou, C., Song, J., Wei, S., et al. (2018), Abundances and light absorption properties of brown carbon emitted from residential coal combustion in China, *Environmental Science & Technology*, *53*(2), 595-603, https://doi:10.1021/acs.est.8b05630
Li, T., Li, J., Jiang, H., Chen, D., Zheng, Z., Chongguo, T., &Gan, Z. (2020), Source Apportionment of PM2.5 in Guangzhou Based on an Approach of Combining Positive Matrix Factorization with the Bayesian Mixing Model and Radiocarbon, *Atmosphere*, *11*(5), 512, https://doi:10.3390/atmos11050512
Lin, P., Aiona, P. K., Li, Y., Shiraiwa, M., Laskin, J., Nizkorodov, S. A., &Laskin, A. (2016), Molecular Characterization of Brown Carbon in Biomass Burning Aerosol Particles, *Environmental Science & Technology*, *50*(21), 11815-11824, https://doi:10.1021/acs.est.6b03024
Lin, Y.-C., Huh, C.-A., Hsu, S.-C., Lin, C.-Y., Liang, M.-C., &Lin, P.-H. (2014), Stratospheric influence on the concentration and seasonal cycle of lower tropospheric ozone: Observation at Mount Hehuan, Taiwan, *Journal of Geophysical Research: Atmospheres*, *119*(6), 3527-3536, https://doi:10.1002/2013jd020736
Liu, G., Wu, J., Li, Y., Su, L., &Ding, M. (2020), Temporal Variations of 7Be and 210Pb Activity Concentrations in the Atmosphere and Aerosol Deposition Velocity in Shenzhen, South China, *Aerosol and Air Quality Research*, *20*(7), 1607–1617, https://doi:10.4209/aaqr.2019.11.0560
Liu, J., Bergin, M., Guo, H., King, L., Kotra, N., Edgerton, E., &Weber, R. J. (2013), Size-resolved measurements of brown carbon in water and methanol extracts and estimates of their contribution to ambient fine-particle light absorption, *Atmospheric Chemistry and Physics*, *13*(24), 12389-12404, https://doi:10.5194/acp-13-12389-2013
Liu, J., Li, J., Zhang, Y., Liu, D., Ding, P., Shen, C., et al. (2014), Source apportionment using radiocarbon and organic tracers for PM2.5 carbonaceous aerosols in Guangzhou, South China: contrasting local- and regional-scale haze events, *Environmental Science & Technology*, *48*(20), 12002-12011, https://doi:10.1021/es503102w
Liu, J., Lin, P., Laskin, A., Laskin, J., Kathmann, S. M., Wise, M., et al. (2016), Optical properties and aging of light-absorbing secondary organic aerosol, *Atmospheric Chemistry and Physics*, *16*(19), 12815-12827, https://doi:10.5194/acp-16-12815-2016
Liu, J., Mo, Y., Ding, P., Li, J., Shen, C., &Zhang, G. (2018), Dual carbon isotopes ((14)C and (13)C) and optical properties of WSOC and HULIS-C during winter in Guangzhou, China, *Science of the Total Environment*, *633*, 1571-1578, https://doi:10.1016/j.scitotenv.2018.03.293
Liu, X., Zhang, Y.-L., Peng, Y., Xu, L., Zhu, C., Cao, F., et al. (2019), Chemical and optical properties of carbonaceous aerosols in Nanjing, eastern China: regionally transported biomass burning contribution, *Atmospheric Chemistry and Physics*, *19*(17), 11213-11233, https://doi:10.5194/acp-19-11213-2019
Mao, S., Li, J., Cheng, Z., Zhong, G., Li, K., Liu, X., &Zhang, G. (2018), Contribution of Biomass Burning to Ambient Particulate Polycyclic Aromatic Hydrocarbons at a Regional Background Site in East China, *Environmental Science & Technology Letters*, *5*(2), 56-61, https://doi:10.1021/acs.estlett.8b00001
Mo, Y., Li, J., Jiang, B., Su, T., Geng, X., Liu, J., et al. (2018), Sources, compositions, and optical properties of humic-like substances in Beijing during the 2014 APEC summit: Results from dual carbon isotope and Fourier-transform ion cyclotron resonance mass spectrometry analyses, *Environmental Pollution*, *239*, 322-331, https://doi:10.1016/j.envpol.2018.04.041
Mo, Y., Li, J., Liu, J., Zhong, G., Cheng, Z., Tian, C., et al. (2017), The influence of solvent and pH on determination of the light absorption properties of water-soluble brown carbon, *Atmospheric Environment*, *161*, 90-98, https://doi:10.1016/j.atmosenv.2017.04.037
Mok, J., Krotkov, N. A., Arola, A., Torres, O., Jethva, H., Andrade, M., et al. (2016), Impacts of brown carbon from biomass burning on surface UV and ozone photochemistry in the Amazon Basin, *Scientific Reports*, *6*, 36940, https://doi:10.1038/srep36940
Nguyen, T. B., Laskin, A., Laskin, J., &Nizkorodov, S. A. (2013), Brown carbon formation from ketoaldehydes of biogenic monoterpenes, *Faraday Discussions*, *165*, 473, https://doi:10.1039/c3fd00036b
Norris, G., Duvall, R., Brown, S., &Bai, S. (2014), EPA Positive Matrix Factorization (PMF) 5.0 Fundamentals and User Guide Prepared for the US Environmental Protection Agency Office of Research and Development, *Washington, DC*,
Olson, M. R., Mercedes, V. G., Michael, A. R., Paul, V. R., Mark, A. D., Michael, B., &James, J. S. (2015), Investigation of black and brown carbon multiple-wavelength-dependent light absorption from biomass and fossil fuel combustion source emissions, *Journal of Geophysical Research: Atmospheres*, *120*, https://doi:10.1002/2014JD022970
Qin, Y. M., Tan, H. B., Li, Y. J., Li, Z. J., Schurman, M. I., Liu, L., et al. (2018), Chemical characteristics of brown carbon in atmospheric particles at a suburban site near Guangzhou, China, *Atmospheric Chemistry and Physics*, *18*(22), 16409-16418, https://doi:10.5194/acp-18-16409-2018

Qin, Y. M., Tan, H. B., Li, Y. J., Schurman, M. I., Li, F., Canonaco, F., et al. (2017), Impacts of traffic emissions on atmospheric particulate nitrate and organics at a downwind site on the periphery of Guangzhou, China, *Atmospheric Chemistry and Physics*, *17*(17), 10245-10258, https://doi:10.5194/acp-17-10245-2017
Ramanathan, V., Chung, C., Kim, D., Bettge, T., Buja, L., Kiehl, J. T., et al. (2005), Atmospheric brown clouds: impacts on South Asian climate and hydrological cycle, *Proceedings of the National Academy of Sciences of the United States of America*, *102*(15), 5326-5333.,
Ramanathan, V., Li, F., Ramana, M. V., Praveen, P. S., Kim, D., Corrigan, C. E., et al. (2007), Atmospheric brown clouds: Hemispherical and regional variations in long-range transport, absorption, and radiative forcing, *Journal of Geophysical Research*, *112*(D22), https://doi:10.1029/2006jd008124
Rizzo, L. V., Correia, A. L., Artaxo, P., Procópio, A. S., &Andreae, M. O. (2011), Spectral dependence of aerosol light absorption over the Amazon Basin, *Atmospheric Chemistry and Physics*, *11*(17), 8899-8912, https://doi:10.5194/acp-11-8899-2011
Sengupta, D., Samburova, V., Bhattarai, C., Kirillova, E., Mazzoleni, L., Iaukea-Lum, M., et al. (2018), Light absorption by polar and non-polar aerosol compounds from laboratory biomass combustion, *Atmospheric Chemistry and Physics*, *18*(15), 10849-10867, https://doi:10.5194/acp-18-10849-2018
Shen, Z., Lei, Y., Zhang, L., Zhang, Q., Zeng, Y., Tao, J., et al. (2017a), Methanol Extracted Brown Carbon in PM2.5 Over Xi'an, China: Seasonal Variation of Optical Properties and Sources Identification, *Aerosol Science and Engineering*, https://doi:10.1007/s41810-017-0007-z
Shen, Z., Zhang, Q., Cao, J., Zhang, L., Lei, Y., Huang, Y., et al. (2017b), Optical properties and possible sources of brown carbon in PM2.5 over Xi'an, China, *Atmospheric Environment*, *150*, 322-330, https://doi:10.1016/j.atmosenv.2016.11.024
Stohl, A., Andrews, E., Burkhart, J. F., Forster, C., Herber, A., Hoch, S. W., et al. (2006), Pan-Arctic enhancements of light absorbing aerosol concentrations due to North American boreal forest fires during summer 2004, *Journal of Geophysical Research*, *111*(D22), https://doi:10.1029/2006jd007216
Szidat, S. (2009), Sources of Asian Haze, *Science*, *323*(5913), 470, https://doi:10.1126/science.1169407
Wang, Q., Han, Y., Ye, J., Liu, S., Pongpiachan, S., Zhang, N., et al. (2019a), High Contribution of Secondary Brown Carbon to Aerosol Light Absorption in the Southeastern Margin of Tibetan Plateau, *Geophysical Research Letters*, *46*(9), 4962-4970, https://doi:10.1029/2019gl082731
Wang, Q., He, X., Huang, X. H. H., Griffith, S. M., Feng, Y., Zhang, T., et al. (2017a), Impact of Secondary Organic Aerosol Tracers on Tracer-Based Source Apportionment of Organic Carbon and PM2.5: A Case Study in the Pearl River Delta, China, *ACS Earth and Space Chemistry*, *1*(9), 562-571, https://doi:10.1021/acsearthspacechem.7b00088
Wang, Q., Ye, J., Wang, Y., Zhang, T., Ran, W., Wu, Y., et al. (2019b), Wintertime Optical Properties of Primary and Secondary Brown Carbon at a Regional Site in the North China Plain, *Environmental Science & Technology*, https://doi:10.1021/acs.est.9b03406
Wang, Q. Q., Huang, X. H. H., Zhang, T., Zhang, Q., Feng, Y., Yuan, Z., et al. (2015), Organic tracer-based source analysis of PM 2.5 organic and elemental carbon: A case study at Dongguan in the Pearl River Delta, China, *Atmospheric Environment*, *118*, 164-175, https://doi:10.1016/j.atmosenv.2015.07.033
Wang, X., Heald, C. L., Ridley, D. A., Schwarz, J. P., Spackman, J. R., Perring, A. E., et al. (2014), Exploiting simultaneous observational constraints on mass and absorption to estimate the global direct radiative forcing of black carbon and brown carbon, *Atmospheric Chemistry and Physics*, *14*(20), 10989-11010, https://doi:10.5194/acp-14-10989-2014
Wang, X., Zong, Z., Tian, C., Chen, Y., Luo, C., Li, J., et al. (2017b), Combining Positive Matrix Factorization and Radiocarbon Measurements for Source Apportionment of PM2.5 from a National Background Site in North China, *Scientific Reports*, *7*(1), 10648, https://doi:10.1038/s41598-017-10762-8
Wang, Y., Hu, M., Guo, S., Wang, Y., Zheng, J., Yang, Y., et al. (2018), The secondary formation of organosulfates under interactions between biogenic emissions and anthropogenic pollutants in summer in Beijing, *Atmospheric Chemistry and Physics*, *18*(14), 10693-10713, https://doi:10.5194/acp-18-10693-2018
Wang, Y., Hu, M., Lin, P., Tan, T., Li, M., Xu, N., et al. (2019c), Enhancement in Particulate Organic Nitrogen and Light Absorption of Humic-Like Substances over Tibetan Plateau Due to Long-Range Transported Biomass Burning Emissions, *Environmental Science & Technology*, *53*(24), 14222-14232, https://doi:10.1021/acs.est.9b06152
Washenfelder, R. A., Attwood, A. R., Brock, C. A., Guo, H., Xu, L., Weber, R. J., et al. (2015), Biomass burning dominates brown carbon absorption in the rural southeastern United States, *Geophysical Research Letters*, *42*(2), 653-664, https://doi:10.1002/2014gl062444

Wu, G., Ram, K., Fu, P., Wang, W., Zhang, Y., Liu, X., et al. (2019), Water-soluble Brown Carbon in Atmospheric Aerosols from Godavari (Nepal), A Regional Representative of South Asia, *Environmental Science & Technology*, *53* (7), 3471-3479, https://doi:10.1021/acs.est.9b00596
Xie, M., Chen, X., Hays, M. D., &Holder, A. L. (2019a), Composition and light absorption of N-containing aromatic compounds in organic aerosols from laboratory biomass burning, *Atmospheric Chemistry and Physics*, *19*(5), 2899-2915, https://doi:10.5194/acp-19-2899-2019
Xie, M., Chen, X., Hays, M. D., Lewandowski, M., Offenberg, J., Kleindienst, T. E., &Holder, A. L. (2017a), Light Absorption of Secondary Organic Aerosol: Composition and Contribution of Nitroaromatic Compounds, *Environmental Science & Technology*, *51*(20), 11607-11616, https://doi:10.1021/acs.est.7b03263
Xie, M., Chen, X., Holder, A. L., Hays, M. D., Lewandowski, M., Offenberg, J. H., et al. (2019b), Light absorption of organic carbon and its sources at a southeastern U.S. location in summer, *Environmental Pollution*, *244*, 38-46, https://doi:10.1016/j.envpol.2018.09.125
Xie, M., Hays, M. D., &Holder, A. L. (2017b), Light-absorbing organic carbon from prescribed and laboratory biomass burning and gasoline vehicle emissions, *Scientific Reports*, *7*(1), 7318, https://doi:10.1038/s41598-017-06981-8
Yan, C., Zheng, M., Bosch, C., Andersson, A., Desyaterik, Y., Sullivan, A. P., et al. (2017), Important fossil source contribution to brown carbon in Beijing during winter, *Scientific Reports*, *7*, 43182, https://doi:10.1038/srep43182
Yan, C., Zheng, M., Sullivan, A. P., Bosch, C., Desyaterik, Y., Andersson, A., et al. (2015), Chemical characteristics and light-absorbing property of water-soluble organic carbon in Beijing: Biomass burning contributions, *Atmospheric Environment*, *121*, 4-12, https://doi:10.1016/j.atmosenv.2015.05.005
Yan, C., Zheng, M., Sullivan, A. P., Shen, G., Chen, Y., Wang, S., et al. (2018), Residential Coal Combustion as a Source of Levoglucosan in China, *Environmental Science & Technology*, *52*(3), 1665-1674, https://doi:10.1021/acs.est.7b05858
Yan, F., Kang, S., Li, C., Zhang, Y., Qin, X., Li, Y., et al. (2016), Concentration, sources and light absorption characteristics of dissolved organic carbon on a medium-sized valley glacier, northern Tibetan Plateau, *The Cryosphere*, *10*(6), 2611-2621, https://doi:10.5194/tc-10-2611-2016
Yu, X., Li, D., Li, D., Zhang, G., Zhou, H., Li, S., et al. (2020), Enhanced Wet Deposition of Water-Soluble Organic Nitrogen During the Harvest Season: Influence of Biomass Burning and In-Cloud Scavenging, *Journal of Geophysical Research: Atmospheres*, *125*(18), e2020JD032699, https://doi:10.1029/2020jd032699
Zhang, Q., Shen, Z., Zhang, L., Zeng, Y., Ning, Z., Zhang, T., et al. (2020), Investigation of Primary and Secondary Particulate Brown Carbon in Two Chinese Cities of Xi'an and Hong Kong in Wintertime, *Environmental Science & Technology*, *54*(7), 3803-3813, https://doi:10.1021/acs.est.9b05332
Zhang, Y.-L., El-Haddad, I., Huang, R.-J., Ho, K.-F., Cao, J.-J., Han, Y., et al. (2018), Large contribution of fossil fuel derived secondary organic carbon to water soluble organic aerosols in winter haze in China, *Atmospheric Chemistry and Physics*, *18*(6), 4005-4017, https://doi:10.5194/acp-18-4005-2018
Zheng, G., Sedlacek, A. J., Aiken, A. C., Feng, Y., Watson, T. B., Raveh-Rubin, S., et al. (2020), Long-range transported North American wildfire aerosols observed in marine boundary layer of eastern North Atlantic, *Environment International*, *139*, 105680, https://doi:10.1016/j.envint.2020.105680
Zhu, C. S., Cao, J. J., Huang, R. J., Shen, Z. X., Wang, Q. Y., &Zhang, N. N. (2018), Light absorption properties of brown carbon over the southeastern Tibetan Plateau, *Science of the Total Environment*, *625*, 246-251, https://doi:10.1016/j.scitotenv.2017.12.183
Zhu, S., Ding, P., Wang, N., Shen, C., Jia, G., &Zhang, G. (2015), The compact AMS facility at Guangzhou Institute of Geochemistry, Chinese Academy of Sciences, *Nuclear Instruments and Methods in Physics Research B*, *361*, 72-75, https://doi:10.1016/j.nimb.2015.06.040
Zong, Z., Wang, X., Tian, C., Chen, Y., Qu, L., Ji, L., et al. (2016), Source apportionment of PM2.5 at a regional background site in North China using PMF linked with radiocarbon analysis: insight into the contribution of biomass burning, *Atmospheric Chemistry and Physics*, *16*(17), 11249-11265, https://doi:10.5194/acp-16-11249-2016